



Final Draft of the original manuscript

Caggiu, L.; Iacomini, A.; Pistidda, C.; Farina, V.; Senes, N.; Cao, H.; Gavini, E.; Mulas, G.; Garroni, S.; Enzo, S.:

In situ synchrotron radiation investigation of V₂O₅–Nb₂O₅ metastable compounds: transformational kinetics at high temperatures with a new structural solution for the orthorhombic V₄Nb₂O₆0 phase.

In: Dalton Transactions. Vol. 49 (2020) 48, 17584 – 17593.

First published online by RSC: 09.11.2020

<https://dx.doi.org/10.1039/d0dt03426f>

In-situ Synchrotron radiation investigation of the V₂O₅-Nb₂O₅ metastable compounds: kinetics transformations at high temperatures with new structure solution for orthorhombic V₄Nb₂₀O₆₀ phase.

Laura Caggiua*, Antonio Iacominia, Claudio Pistiddab, Valeria Farinaa, Nina Senes, Hujun Caob, Elisabetta Gavinia, Gabriele Mulasa, Sebastiano Garronia, Stefano Enzoa*

Abstract

Due the high interest addressed versustowards vanadium niobium oxides as lithium storage material, the kinetics and transformation processes of the V₂O₅-Nb₂O₅ system have been investigated by in situ synchrotron powder X-ray diffraction. The diffraction data after thermal treatments selected in correspondence of significant features, were supplemented with specific off-situ experiments conducted with a laboratory rotating anode X-ray laboratory sourcediffractometer. The morphological changes of the mixed powders assuming amorphous and nano-crystalline solid solution structure as a function of temperature, were inspected with scanning electron microscopy observations. A The structural solution from of the powder diffraction pattern of the phase recorded in situ in theat a temperature range aroundof about 700 °C has supplied theis compatible with an orthorhombic crystal structure of space group Amm2 space group proposal with atomic location in the unit cell compatible with accurately determined experimental density. Our results suggest Tthe obtained lattice parameters for this structure are $a = 3.965 \text{ \AA}$; $b = 17.395 \text{ \AA}$; $c = 17.742 \text{ \AA}$, and the cell composition V₄Nb₂₀O₆₀, Pearson symbol oA84, density = 4.10 g/cm³. In this structure, while niobium atoms may be four, five and six-fold coordinated by oxygen atoms, the vanadium atoms are six-fold or seven-fold coordinated, respectively. At the temperature of 800 °C and nearly above, the selected 1:2 and 1:3 V₂O₅-Nb₂O₅ compositions respectively returned mostly a tetragonal VNb₉O₂₅ phase, in line with earlier observations conducted for determination of the stability phase diagram of such quasi-binary system.

1. Introduction

For more than one decade, Vanadium pentoxide (V₂O₅) has played an important role as electrode in lithium-ion batteries due to its interesting performances and peculiar crystalline structure1–8. Very Recently, promising results in terms of enhanced electronic conductivity, higher specific capacity, lower capacity loss and better cyclability, have been achieved by combining V₂O₅ with Nb9–12, shifting the interest versus towards the synthesis of vanadium niobium oxides as lithium storage material. In particular, the ternary oxide defined as “V₄Nb₁₈O₅₅” exhibited a lithium uptake capacity of 221 mA h g⁻¹ higher than the most exploited Li₄Ti₅O₁₂ (165 mA h g⁻¹) in the same working window9.

Since the pioneering study in the late 1965 by Waring and Roth13 which described the phase equilibria in the vanadium oxide-niobium oxide system, an appreciable progress has been made in the determination of the crystal structure of “V₄Nb₁₈O₅₅” compound which is a composition located close to the Nb₂O₅ rich branch. Yamaguchi et al.14 synthesized the system starting from the respective alkoxides mixed in a molar V:Nb ratio of 2:9 and thermally annealed at 630 °C. The final phase was associated with a compound with orthorhombic geometry, chemical formula V₄Nb₁₈O₅₅ and lattice parameters $a = 7.939$, $b = 17.3100$; $c = 17.610 \text{ \AA}$. However, any no space group was provided by in this investigation. Further indexing studies15 established that the a-axis

parameter may be halved, that is $a = 3.967 \text{ \AA}$. Borrnert et al.¹⁶, in order to reconcile preliminary single-crystal experiments where the Cmmm space group was surmised, proposed to solved the crystal structure of the diffraction pattern pattern of a obtained from a phase of mixture of supposed assumed composition V4Nb18O55, obtained from freeze-drying precursors, as reported by Mayer-Uhma (PhD Thesis)¹⁷.

After inspecting the CIF file proposed by Borrnert et al.¹⁶, it can be assessed that some interatomic distances turn out to be unacceptably short. Moreover, the structure work proposed by Qian et al.¹⁸, reported again with a V4Nb18O55 composition, supplied a CIF file that cannot be satisfactory to reproduce the previously reported diffraction pattern.

As it emerged from the above-mentioned literature, the crystal structure of “V4Nb18O55” still remains hotly debated if not obscure. This might be due to the fact that , maybe because its chemical composition has never been assessed and validated completely. This overview suggested to reconsider from the beginning the diffraction pattern first reported by Yamaguchi et al.¹⁴ and acquired in the PDF card #46-0087, also in view of the progresses reached in the field of structure solutions from powder diffraction data made available with suitable software.

The correlation between the determined experimental density with the space group and atomic location in the unit cell of the phase analyzed, is an obliged step to acquire a full and accurate description of the crystal structure.

With the aim to shed light on this aspect, we investigated, in detail, the structural transformation emerged on the vanadium and niobium oxides mixed in a molar ratio 1:5. The final system was obtained by a solid state route combining mechanochemical and thermal treatments. The structural evolution as a function of the temperature has been studied by X-ray diffraction collected in laboratory and synchrotron facilities, while morphology insights have been determined by scanning electron microscopy coupled with EDS. The structure of the crystallization product from the mixture V2O5·5Nb2O5 BM ball milled (BM) for 24 h was finally solved by combining experimental density supplied by pycnometer apparatus with X-ray powder diffraction data.

2. Experimental

The starting reagents, V2O5 (purity 99.99%) and Nb2O5 (purity 99.99%) powders, were purchased from Alfa Aesar.

The mechanical treatment was carried out by a SPEX mix/miller mod. 8000 working at 875 rpm. 4 grams of powders composed by V2O5 and Nb2O5 mixture (1:5) were inserted into a steel vial and then charged with 2 stainless steel balls of 4 g each one. Further experiments were conducted changing the stoichiometric molar ratio of the starting reagents, specifically: 1:2 and 1:3. All the milling treatments were performed for 24 h and the as-milled products were subsequently thermally annealed for 2 h, at different selected temperatures (500 °C, 600 °C, 700 °C and 800 °C), in a horizontal muffle (Ney 2-525).

A Rigaku SmartLab X-ray powder Diffractometer, aligned according to the Bragg–Brentano geometry with a rotating Cu anode ($\text{K}\alpha$ radiation $\lambda = 1.54178 \text{ \AA}$) and a graphite monochromator in the diffracted beam, was employed to acquire diffraction pattern of the different synthesized powders. The evaluation of the XRD powder patterns started using ‘HighScore’¹⁹ to identify the known crystallographic structures and the phases evolution in function of the stoichiometric ratio and annealing temperature. The patterns were further refined according to the Rietveld method^{20,21},

using the MAUD (Materials Analysis Using Diffraction)22 software. The refinement procedure allowed us to highlight the structure and microstructural dissimilarities between the milled samples, before and after the heat treatment. From the unclassified peak sequence in the patterns, it was possible to find the lattice parameter values using the McMaille and Dicvol indexing programs^{23,24}. The information acquired by these software were combined with the isolated compound density value, obtained using a gas pycnometer (AccuPyc II 1340). To inspect possible structure solutions for cell devised after indexing we used the Endeavour program²⁵.

In situ synchrotron radiation powder X-ray diffraction (SR-PXD) technique was applied using a specially designed cell²⁶. This cell with sapphire capillary allows to collect X-ray diffraction patterns under controlled gas atmosphere in a pressure range from 0.01 to 200 bar . Measurements were performed at Deutsches Elektronen-Synchrotron (DESY) at the P02.1 station. The beamline with X-ray source of 60 keV ($\lambda = 0.2111 \text{ \AA}$) was equipped with a Perkin Elmer XRD1621 area detector. The powder was heated from room temperature (RT) to 825 °C with a heating rate of 5 °C/min under 1 bar of Ar pressure. A two-dimensional SR-PXD pattern was collected every 10 s. The 2D data were integrated and reduced to one-dimensional diffraction pattern using Fit2D software²⁷ having care to avoid the single-crystal spots due to sapphire.

Morphological observations of the as milled and annealed powders were conducted by scanning electron microscopy (FEI Quanta 200 instrument).

3. Result and discussion

We examine first the diffraction data undertaken acquired on the a powders mixing mixture of V₂O₅ and Nb₂O₅ in the molar ratios 1: 5. The parental purchased powders (i.e. V₂O₅ and Nb₂O₅) were reported by the supplier with a high degree of purity but not documentedno information with XRD patternson the material crystal structures were provided. As it is reported in figure 1 for the 1:5 mixture, our phase analysis assessed that the Nb₂O₅ compound is monoclinic, space group P2/m, lattice parameters $a = 21.187 \text{ \AA}$; $b = 3.827$; $c = 19.377$ and $\beta = 119.83^\circ$, respectively, while V₂O₅ is of orthorhombic geometry, space group Pmnm, $a = 11.521 \text{ \AA}$; $b = 4.376 \text{ \AA}$ and $c = 3.567 \text{ \AA}$, respectively.

Fig. 1 The XRD patterns (laboratory equipment) of the V₂O₅-Nb₂O₅ mixture 1:5 before (bottom pattern) and after (top) ball milling for 24 h. The top pattern is typical of a semicrystalline system, i.e., made simultaneously by micro-(nano-)crystalline component (orthorhombic geometry, violet line) and amorphous (dark cyan line). In both patterns the background estimated with a polynomial is reported as green line. The bar sequence at the bottom is the peak location progression expected for the two oxide compounds based on the space group of relevant crystallographic phases.

The bBall milling for 24 h of the starting mixtures mixture for 24 hours leads to a semicrystalline system, i.e., an amorphous component plus a (nano)-crystalline phase. The “crystallinity” intended as the amount of crystal phases with respect to the total amount including the otherwise amorphous component,²⁸ is estimated to be roughly 38.0 wt %.

The sequence of Bragg peaks presented in the XRD diagram of the as-milled system, is very similar for intensity progression to the pattern reported in the literature as «pseudo-hexagonal» form of

Nb₂O₅ 29. The lattice parameters for the “pseudo-hexagonal” Nb₂O₅-like phase ($a = 3.607$; $c = 3.925$ Å) are referring to a cell volume $V = 44.22$ Å³ which may accommodate half stoichiometric unit of the Nb₂O₅ “molecule”. However, the diffraction pattern of this form can be fitted satisfactorily (see Figure 1) using the Pbam orthorhombic space group (violet line)³⁰ known for a Nb₂O₅ modification ($\rho = 4.98$ g/cm³). Thus, our nano-crystalline phase is very likely a solid solution, written formally as (Nb_xV_{1-x})₂O₅, which can be also indicated as M₂O₅, where M is identified with Nb and V. Therefore, the expected crystallographic density values of 4.99 and/or 4.98 g/cc calculated on the basis of the vanadia/niobia molecular units in the cell volume, should be lowered to 4.72 g/cm³ for the M₂O₅ mixtures 1:5. For comparison purposes, note that the density of the 1:1 VN₂O₅ crystalline compound³¹ was reported to be 3.27 g/cm³.

The considerable line broadening evaluable for of the crystalline component may be caused by the overlapping of nearby peaks due to the close sequence of hkl peaks related to the lattice parameter values of the Pbam space group, as well as by reduced crystallite size and by the increased lattice disorder increase effects³². Note It is important to notice that after the initial calibration, the Rietveld program adopted³³ incorporates the instrument broadening. Accordingly, the fit parameters of the line broadening obtained directly at the end of the numerical iterations, suggest that the average crystallite size value for the processed powders investigated sample is around 250 Å (± 20), while the lattice strain average content is close to 0.002 (± 0.0005) for the mixture ratio here considered.

The 2-D plot reported in Figure 2, seems to confirm that the mixture of the amorphous and nanocrystalline phases obtained upon milling remain relatively stable until 450 °C. For At higher temperature, the grain coarsening of the nanocrystalline phase takes place, while the removal disappearance of the amorphous component material fraction can be surmised and detected at 500 °C. At higher temperatures (> 640 °C), significant phases transformations occur, which can be related with formation of new solid products.

Fig. 2 2-D plot of the 1:5 mixture ball milled for 24 h and subjected to the thermal treatment from RT up to 830 °C. The six remaining horizontal lines (from bottom to the top respectively) are in correspondence of significant thermal events and transformations

Starting from the 1-D pattern (Figure 3) at the beginning of the heating experiment, it emerges that the signal-to-background ratio is affected by the capillary glass which, on the other hand, is necessary to warrant the constant exposition of the powder volume with respect to the incoming beam. In particular, we can easily surmise that the crystallization of the amorphous component (halo located approx. at 2.0 Å⁻¹) produced after ball milling, presumably overlapped also by the amorphous contribution of the glass capillary, is persisting until temperatures around 500 °C, as it emerges from the analysis of selected 1-D patterns reported in Figure 3. Note the increased intensity and peak-sharpening effected by the temperature treatment, witnessing increase of the average crystallite size and/or lattice strain decrease.

Fig. 3 1-D X-ray diffraction patterns acquired at 40 °C, 450 °C and 550 °C during the in-situ experiment performed at DESY.

In order to proceed with a deep analysis of the other phases involved in the chemical process, room temperature XRD patterns were acquired on the powders post annealed at 500 °C, 600 °C, 700 °C and 800 °C, respectively. In fact, from one hand the use of a plate image enabled fast acquisition of patterns with excellent signal-to-noise ratio, thus making possible to follow transformation processes, on the other hand the presence of a graphite monochromator in the diffracted beam (laboratory equipment) avoids the capillary contribution to the total scattering, allowing better signal-to-background ratio.

In Figure 4 we examine the effect of the temperature on the ball-milled powders (selected 1:5 composition). The diffraction pattern acquired for the material treated at 500 °C for 2 hours shows a clear reduction of the material amorphous component. Starting from room temperature, the amorphous component is going to disappear after a thermal treatment at 500 °C for 2 h, in analogy to agreement with the previously reported XRD experiment. In fact,, to the point that the pattern was fitted just simply using the Pbam (pseudo-hexagonal) orthorhombic phase after refining the fractional coordinates of atoms referred to general positions. The structure seems to remain unchanged until 600 °C but, due to a couple of weak peaks at 26.9° and 31.1°, might suggest the beginning of it may be suggestion for early stages of an additional phase development. As a matter of fact, the pattern collected after the thermal treatment at 700 °C (holding time 2 h) refers to a new phase, having a peak sequence similar to that reported by Yamaguchi et al.¹⁴, see also recorded card #46-0087 (PDF4 database- ICDD). These data were associated to a compound with orthorhombic geometry, chemical formula Nb₁₈V₄O₅₅ and lattice parameters $a = 7.939 \text{ \AA}$, $b = 17.310 \text{ \AA}$; $c = 17.610 \text{ \AA}$, respectively. Further indexing studies¹⁵ established that the a-axis parameter may be halved, that is $a = 3.967 \text{ \AA}$. Börrnert et al.¹⁶, in order to reconcile preliminary single-crystal experiments where the Cmmm space group was surmised, proposed to solve the pattern of a mixture of supposed composition V₄Nb₁₈O₅₅, obtained from freeze-drying precursors, as reported by Mayer-Uhma¹⁷(PhD Thesis). We anticipate here that a better space group where to develop a sensible structure solution may be also Amm2 n.38 in IT. Finally, after treatment at 800 °C, the top pattern is material crystal structure can be easily attributed to the VNb₉O₂₅ tetragonal phase, space group I4/m , refined lattice parameters $a = 15.704 \text{ \AA}$; $c = 3.812 \text{ \AA}$, respectively³⁴.

Fig. 4 The XRD patterns (laboratory equipment) of the 1-to-5 V/Nb molar mixture ball milled for 24 h and subjected to ex-situ thermal annealing (holding time 2 h) at the indicated temperatures.

As it concerns the morphological characterization, it was observed by SEM that the as-milled powder sample consisted of particle aggregates with wide a size distribution of dimensions in the range 2-20 µm (Figure 5 a1). Magnification of a single agglomerate (Figure 5 a2) highlights two different morphologies referred to two different scales of aggregations. Similar information can be visualized in Figure 5 b1 and b2 for the powders annealed at 600 °C. On the other hand, the micrographs acquired for the powders heated at 700 °C (Figure 5 c1 and c2) seems to be composed by smaller particles (from 0.2 to 3 µm). This morphologically analysis highlights the differences emerged in literature following other synthetic procedures. The powders synthesized by ball milled milling, as in this case, appear dustiest more powdery compared to those , that are more orderly organized, which were obtained following wet-chemistry protocols^{9,18}. For the samples treated at higher On increasing the temperature, the differences ascribable to the different synthesis methods tend to be attenuated, until vanishing in Figure 5 d1 and d2 for the powders obtained at 800 °C.

Here, the powder morphology is characterized by the presence of rods with average size of 4 μm , which is in agreement with observations reported previously by other groups^{10,35,36}. Schadow et al.³⁵ were the first to report rod-like shapes for the VNb9O25 phase, although SEM images with similar shape were also reported by Bergner et al.³⁶. Furthermore, more recently Fu et al.¹⁰, have studied the tetragonal I4/m “V3Nb17O50” compound after treatment at 800–950 °C, invariably observing rods with size distribution located in the range 3–8 μm .

Fig. 5 SEM micrographs of the 1-to-5 molar mixture ball milled for 24 h and subjected to ex-situ thermal annealing (holding time 2 h) at the indicated temperatures. a) as milled, b) 600 °C, c) 700 °C, d) 800 °C.

To correctly address a structure solution for the powder pattern observed for the first time by Yamaguchi et al.¹⁴, the first issue to be considered is connected to the true chemical composition of the underlying compound, initially suspected as 2V2O5·9Nb2O5. In principle the number of “generic” molecular units M2O5 would be likely even and not odd (for example 12, but we cannot reject 10), because of the site multiplicities involved in the isometric system. Having 10, 11 or 12 molecular units to allocate in a unit cell volume of ca 1220 \AA^3 is making some sensible difference in the resulting crystallographic density value.

Nevertheless, the expected chemical composition may be confirmed from by experimental density evaluation. Our We determination determined for the 1:5 powdered sample treated at 700 °C returned a density value of $4.12 \text{ g/cm}^3 \pm 0.05$. This indicates that the composition in the unit cell of volume 1220 \AA^3 might be better V4Nb20O60 (equivalent to $\rho = 4.09 \text{ g/cm}^3$) rather than V4Nb18O55, as initially surmised by Yamaguchi et al.¹⁴, a composition leading for this cell to $\rho = 3.72 \text{ g/cm}^3$. Specifically, in Figure 6, we report (data points) the crystallographic density values determined for the so far resolved phases: pure V2O5 ($\rho = 3.36 \text{ g/cm}^3$), equimolar VNbO5 ($\rho = 3.272$), tetragonal VNb9O25 ($\rho = 4.475$) and monoclinic Nb2O5 ($\rho = 4.6 \text{ g/cm}^3$). Note It must be mentioned that our pycnometer and crystallographic density evaluations agree within experimental uncertainty and can be represented by the Pearson symbol oA84. The value surmised for the V4Nb20O60 composition falls along a “ideal” smooth line connecting the individual density of various solved structures. Also reported in Figure 6 are the crystal density expected from the chemical composition surmised by Yamaguchi et al.¹⁴, (oP77 in red) and the analogous value coming from the structure solution proposed by Börrnert et al.¹⁶ (erroneously reported in their reference to be 6.02 g/cm^3 but actually evaluated from site occupation being 4.62 g/cm^3). Even from this point of view of the density curve intercepted for the V2O5-Nb2O5 system, some oddities of the assumed structure can be suspected, ascribable to imperfect attributions in previous determinations.

The crystal structure of “single-phase” vanadia, “single-phase” niobia and tetragonal VNb9O25, were determined from single crystal methods, while space group and crystal structure of VNbO5 and 4(VNb5O15) of the present investigation, respectively, were solved from the powder patterns made available by laboratory and synchrotron station diffractometers in the reflection and transmission mode, respectively.

Fig. 6 The density behavior (full line) across the V2O5-Nb2O5 composition for the known crystallographic compounds. The equimolar compound is lighter than pure V2O5 while for pure Nb2O5, various polymorphic values are reported in the literature in a range from 4.60 to 5.00 g/cm^3 . It is observed that the density value calculated from data of ref. 14 below an expectation line (navy

curve) traced to connect the data points smoothly. Also, the effective density assumed by Börrnert et al. appears too high, while the value proposed for a 1:5 mixture with chemical formula (VNb₅O₁₅)₄ seems to be adequate.

Concerning the products prepared starting by mixing V₂O₅ and Nb₂O₅ powders in the molar ratio 1:5 subjected to 24 h of ball milling and treated at 700 °C, the synchrotron and laboratory X-ray powder patterns are compared in Figure 7, where the intensities are shown in log scale after normalizing diffraction angles to the associated reciprocal space variable Q (Å⁻¹ units). The experimental data points (blue) are fit according to Le Bail method 24 (red line). In the comparison we can evaluate the pros and cons of the off-situ laboratory data collection with the Bragg-Brentano reflection geometry and a monochromator in the diffracted beam vs the in-situ synchrotron radiation, where the pattern is obtained after integrating the concentric rings of the 2-D plate-image detector, with the advantage of a good signal-to-noise ratio, but with the penalty of a lower signal-to-background ratio.

Fig. 7 Comparison between the synchrotron radiation experiment after annular integration of the 2-D plate image (top) and XRD laboratory equipment pattern (bottom) plotted vs the reciprocal space variable Q, as indicated by inside legends. The presence of a graphite monochromator in the diffracted beam (laboratory equipment) allows better signal-to-background ratio. However, the use of a plate image enables fast acquisition of patterns with excellent signal-to-noise ratio, thus making possible to follow carefully transformation processes.

The bar sequence at the bottom are locating expected peak positions on the basis of lattice parameter values and space group generated hkl. Small differences from the line positions of the two patterns, if any, are relatable related to their different temperature (in-situ 700 °C vs ex-situ RT) during the data collection experiments, respectively. In fact, both patterns were submitted to indexing according to the McMaille23 program and supplied similar values for the lattice parameters (see table 1), determined according to orthorhombic system:

$\lambda / \text{\AA}$ a / Å b / Å c / Å V / Å³

700 °C in-situ synchrotron expt 0.2111 3.972 17.471 17.742 1231.2

RT XRD laboratory expt 1.5418 3.974 17.406 17.715 1225.4

Tab.1 The lattice parameter values determined according to McMaille from the peak sequence of the two patterns reported in Figure 7. While the unit cell volumes are similar, the intermediate b-

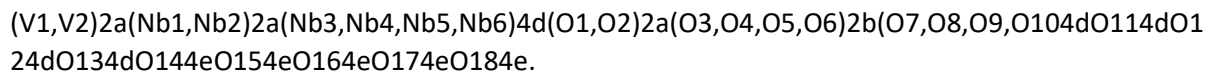
axis value shows the larger discrepancy. This might be ascribed, at least partially, to the different situation during data collection for the two experiments.

i) Chemical Formula.

Such data represent a confirmation of the indexing proposed first by Tabero et al.¹⁵, although the unit cell volume is slightly larger than that determined from the stick pattern of Yamaguchi et al.¹⁴. In addition, from the initial mixture ratio used 1:5 and density evaluation, we may consider assume that the chemical composition of the orthorhombic phase is VNb₅O₁₅ with Z = 4.

ii) Space group and crystallochemical formula

From the experimental patterns reported in Figure 7, analysis of extinctions and systematic absences using Endeavour25 (simulated annealing program) suggested that the most likely space group may be Amm2 (n. 38) and not Cmmm or Cmm2 as reported by Borrnert et al.¹⁶ and by Qian et al.¹⁸. As for the final crystallochemical formula, the Wyckoff sequence of atomic coordinates does not appear to be a consolidated output, but we have reason to believe that the most likely output is e5d11b4a6. Thus, the proposed crystallochemical formula from the structure solution may be represented as:



iii) Local environment around metal atoms.

Figure 8 depicts a polyhedral representation of the unit cell content determined by Endeavour25. One sees it can be seen that Vanadium atoms are surrounded by 5 Oxygens in a triangular antiprism configuration (hexahedron), while Niobium atoms may have coordination arrangement from almost planar 4-fold, five-fold (hexahedron) and 6-fold (octahedral coordination). This coincides only partially with the results recently reported by Qian et al.¹⁸. A Cmmm space group was employed by these authors according to an effective Pearson representation oC84, which implies a crystal density similar to that supplied by our solution.

Fig. 8 Polyhedral representation of the Amm2 4(VNb₅O₁₅) compound, as solved using Endeavour. The red polyhedras (hexahedra and heptahedra) are vanadium atoms surrounded by oxygens, while the green polyhedra built with oxygen surrounding niobium atoms may be four-fold, five-fold and six-fold coordinated, respectively.

The solution of such structure enables to extract quantitative information on the kinetics observed from in-situ synchrotron radiation experiment reported in term of contour plot image in Figure 2.

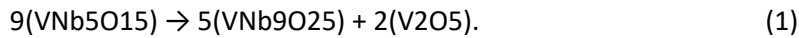
We have also examined in Figure 9 the behavior of the integrated 1-D patterns in correspondence of the temperature range 650-710 °C (4th and 5th horizontal lines in Figure 2).

It can be seen here that the transformation is taking place from the pseudo-hexagonal habit (modified orthorhombic space group Pbam-violet line) to the new orthorhombic Amm2 phase just solved (cyan line).

In practice the transformation is fully accomplished in a range of ca 60 °C during the transformation ramp.

The Amm2 phase is comparatively stable (no significant volume change of the unit cell from lattice parameters evaluation according to Rietveld) for a further temperature increase of 80 °C. In fact, the XRD patterns are remaining the same until T = 760 °C, where a tiny fraction of VNb9O25 tetragonal lattice phase, space group I4/m, measured parameters $a = 15.736 \text{ \AA}$ and $c = 3.815 \text{ \AA}$, respectively, seems to appear. By increasing the temperature until 825 °C, the amount of tetragonal phase increases (52.0 wt%) at expenses of the orthorhombic Amm2 phase. After evaluating the chemical composition of retrieved phases it is evident that the transformation occurring at this stage involves loss of V2O5 molecules, which are difficult, but not impossible, to account in the pattern, although the temperature value is high enough to liquefy this component. In any case, we give in Figure 10 the kinetics even for this transformation, that seems to be in agreement with previous high-temperature studies undertaken with the objective of qualifying the thermal stability of solid solutions rich in Niobium³⁷.

From Figure 10, where the transformation $\text{VNb5O15} \rightarrow \text{VNb9O25}$ is involved, we can define the stoichiometry of the reaction according to the following decomposition on heating (eq. 1):



It is likely that Yamaguchi et al.¹⁴ rather than considering this path, due to the difficulty of observing the decomposed shcherbianite, simply assumed the opposite direction following the phase diagram from the VNb9O25 composition cooling down from high temperature, that is, they speculated the enrichment of two VNb9O25 cells with one V2O5 molecule unit according to the equation $\text{V2Nb18O50} + \text{V2O5} = \text{V4Nb18O55}$. However, as already pointed out, the conjecture supposed in¹⁴ was not assisted by any independent evaluation of the density for the supposed phase, which may have created misunderstanding on the composition. In alternative, it would be interesting to verify with computational methods the stable phases as well as to study reaction pathways.

Fig. 9 The transformation kinetics process from pseudo-hexagonal orthorhombic Pbam (Nb,V) 2O_5 mixture to Amm2 polymorph, where the vanadium atoms are involved in irregular hexahedra with five-fold coordination by oxygen atoms.

Fig. 10 Kinetics details of the transformation occurring at the indicated temperature from a Amm2 space group for the VNb5O15 compound to tetragonal I4/m VNb9O25. The change in composition implies evolution of 2 V2O5 molecules for as many as 5 VNb9O25 chemical formulas transformed.

Of course, nor the Amm2 phase neither the P212121 VNbO5 phases were reported in the most recent thermodynamically assessed V2O5-Nb2O5 phase diagram^{38,39}, where the only stable phase is the peritectic tetragonal I4/m VNb9O25. In fact, slight amount of what seemed a condensation product was also observed in the broken capillary and in the cell walls of the SR station after termination of the experiment.

The view presented above is coherent for explaining the behavior observed in the Figures S1 respectively after extended ball milling and thermal treatments of the 1:2 and 1:3 V2O5-Nb2O5 systems. Specifically, for the 1:2 mixture ratio, the XRD ex-situ experiment after annealing at 500 °C displays occurrence of the pseudo-hexagonal sequence (presumably a solid solution with composition [V0.33Nb0.67]2O5 described with a distorted Pbam space group) and the equimolar P212121 compound (originally attributed to the Pnma space group²). After a further annealing at 600 °C and 700 °C respectively, we observe occurrence of the orthorhombic Amm2 VNb5O15 phase with the P212121 VNbO5 phase. Note that the cyan line component used to represent the VNbO5 phase is weakened going from 600 °C to 700 °C. Finally, after annealing at 800 °C (holding time 2 h) the total occurrence of the VNb9O25 phase is confirmed, which supports the view of V2O5 evolution operating beyond the specific transformation processes.

The 1:3 mixture shows a similar behavior at parity of annealing treatments (Figure S1). Here the amorphous component seems to have resisted to the temperature treatment at 500 °C at least partially. For the temperature treatments of 600 °C and 700 °C, respectively, we observe again the simultaneous occurrence of the Amm2 VNb5O15 phase together with the P212121 VNbO5 phase, the latter in a lower quantity with respect to the corresponding patterns shown, in rough agreement with expectation from the lever rule. Weak traces of V2O5 phase are also appreciable at 800°C suggesting a disproportionation of metastable phases (Amm2 and P212121) eventually evolving to VNb9O25 and V2O5, regardless of the starting reagents ratio.

4. Conclusions

Mixtures of V2O5 and Nb2O5 (1:5) oxide powders ball milled for 24 h may lead to semicrystalline systems, i.e., composed by a metastable amorphous and a nanocrystalline solid solution phase with pseudo-hexagonal lattice arrangement, better describable with modification of the orthorhombic Pbam space group deduced in analogy to a Nb2O5 modification. The as-mixed products once subjected to thermal treatment, evolve in the structure with elimination of the amorphous component, presumably being incorporated in the pseudo-hexagonal solid solution, remaining in the range 450 – 500 °C, approximately. By further heating the Nb2O5-rich products at about 600 °C, the conversion of the pseudo-hexagonal phase is observed in terms of V-Nb-O new products of crystallization. This observation is analogous to previous preparation procedures using soft

chemistry methods after drying and heating of precursors. The structure of the products after crystallization above 600 °C were recognized to be initially a mixture of P212121 orthorhombic VNbO₅ phase and another orthorhombic component, whose structure solution remained controversial. This investigation has ascertained the chemical composition V₂O₅·5Nb₂O₅ for this compound, thanks to the solid-state preparation procedure which allowed easy and precise control of the chemicals without uncertainties deriving from processing of starting precursors in solution. After examining critically the density behavior of known compounds across the composition of the V₂O₅ - Nb₂O₅ system, the structure of the orthorhombic controversial phase of composition 2(V₂O₅·5Nb₂O₅), equivalent to V₄Nb₂O₆₀, was solved from powder diffraction patterns collected both with laboratory equipment after thermal treatments, lattice parameters $a = 3.965 \text{ \AA}$; $b = 17.395 \text{ \AA}$, $c = 17.742 \text{ \AA}$, space group Amm2 (n. 38), Pearson symbol oA84, density = 4.10 g/cm³. In this structure, while niobium atoms may be four, five and six-fold coordinated by oxygen atoms, the vanadium atoms are six-fold or seven-fold coordinated, respectively.

In all diffraction patterns of the various powders mixture (1 : 2, 1 : 3 and 1 : 5) treated at 800 °C, it always emerged the same phase, namely the tetragonal I4/m VNb₉O₂₅, regardless of stoichiometric ratio of reagents. It is very likely that during high temperature treatments some V₂O₅ molecules may evolve in liquid and gaseous forms.

Conflicts of interest

“There are no conflicts to declare”.

Acknowledgements

The authors acknowledge the support of the CeSAR UNISS, Centro Servizi di Ateneo per la Ricerca of the University of Sassari, for making available several instrumental techniques to carry out materials characterization. The activity of L.C. has been supported thanks to Italian Ministry for University and Science by PON-RI scholarship (Programma Operativo Nazionale Ricerca e Innovazione 2014–2020, Fondo Sociale Europeo Regione Autonoma Sardegna) with a special program, within the joint agreement UNICA-UNISS for the PhD in Chemical and Technological Sciences. S.G., S.E., and G.M. acknowledge UNISS for the financial support received within the program “Fondo di Ateneo per la ricerca 2019”.

Notes and references

- 1 Y. Xu, M. Dunwell, L. Fei, E. Fu, Q. Lin, B. Patterson, B. Yuan, S. Deng, P. Andersen, H. Luo and G. Zou, ACS Appl. Mater. Interfaces, 2014, 6, 20408–20413.
- 2 J. Liu, H. Xia, D. Xue and L. Lu, J. Am. Chem. Soc., 2009, 131, 12086–12087.
- 3 H. G. Wang, D. L. Ma, Y. Huang and X. B. Zhang, Chem. - A Eur. J., 2012, 18, 8987–8993.
- 4 Y. Liu, M. Clark, Q. Zhang, D. Yu, D. Liu, J. Liu and G. Cao, Adv. Energy Mater., 2011, 1, 194–202.
- 5 R. Xiao, J. Xie, T. Luo, L. Huang, Y. Zhou, D. Yu, C. Chen and Y. Liu, J. Phys. Chem. C, 2018, 122, 1513–1521.
- 6 Y. Yue and H. Liang, Adv. Energy Mater., 2017, 7, 1–32.
- 7 K. H. Seng, J. Liu, Z. P. Guo, Z. X. Chen, D. Jia and H. K. Liu, Electrochim. commun., 2011, 13, 383–386.

- 8 C. Wang, L. Zhang, M. Al-Mamun, Y. Dou, P. Liu, D. Su, G. Wang, S. Zhang, D. Wang and H. Zhao, *Adv. Energy Mater.*, 2019, 9, 1–9.
- 9 H. Wu, N. Fan, J. Li, Y. Cao, Y. Zhao, K. Wei, Y. Cui and Y. Cui, *Sustain. Energy Fuels*, 2019, 3, 1384–1387.
- 10 Q. Fu, X. Zhu, R. Li, G. Liang, L. Luo, Y. Chen, Y. Ding, C. Lin, K. Wang and X. S. Zhao, *Energy Storage Mater.*, 2020, 30, 401–411.
- 11 C. Jiang, T. Liu, N. Long, X. Cheng, N. Peng, J. Zhang, R. Zheng, H. Yu and J. Shu, *Ceram. Int.*, 2019, 45, 18111–18114.
- 12 S. Qian, H. Yu, L. Yan, H. Zhu, X. Cheng, Y. Xie, N. Long, M. Shui and J. Shu, *ACS Appl. Mater. Interfaces*, 2017, 9, 30608–30616.
- 13 J. L. Waring and R. S. Roth, *J. Res. Natl. Bur. Stand. Sect. A Phys. Chem.*, 1965, 69A, 119.
- 14 O. Yamaguchi, Y. Mukaida and H. Shigeta, *Adv. Powder Technol.*, 1990, 1, 3–12.
- 15 P. Tabero, E. Filipek and M. Piz, *Cent. Eur. J. Chem.*, 2009, 7, 222–227.
- 16 C. Börrnert, W. Carrillo-Cabrera, P. Simon and H. Langbein, *J. Solid State Chem.*, 2010, 183, 1038–1045.
- 17 T. Mayer-Uhma, Von molekularen Precursoren zu Oxidphasen im System V₂O₅/Nb₂O₅, Thesis, Technische Universität Dresden, 2005.
- 18 S. Qian, H. Yu, X. Cheng, R. Zheng, H. Zhu, T. Liu, M. Shui, Y. Xie and J. Shu, *J. Mater. Chem. A*, 2018, 6, 17389–17400.
- 19 T. Degen, M. Sadki, E. Bron, U. König and G. Nénert, *Powder Diffraction*, 2014, 29, S13–S18.
- 20 H. M. Rietveld, *Acta Crystallogr.*, 1967, 22, 151–152.
- 21 H. M. Rietveld, *J. Applied Crystallography*, 1969, 2, 65–71.
- 22 L. Lutterotti, *Nucl. Instruments Methods Phys. Res. Sect. B Beam Interact. with Mater. Atoms*, 2010, 268, 334–340.
- 23 A. Le Bail, *Powder Diffraction*, 2004, 19, 249–254.
- 24 A. Boultif & D. Louer, *J. Applied Cryst.* 2004, 37, 724–731.
- 25 H. Putz, J. C. Schön and M. Jansen, *J. Applied Crystallography*, 1999, 32, 864–870.
- 26 U. Bösenberg, C. Pistidda, M. Tolkihn, N. Busch, I. Saldan, K. Suarez-Alcantara, A. Arendarska, T. Klassen and M. Dornheim, *Int. J. Hydrogen Energy*, 2014, 39, 9899–9903.
- 27 A. P. Hammersley, *J. Applied Crystallography*, 2016, 49, 646–652.
- 28 W. Ruland, *Acta Crystallogr.*, 1961, 14, 1180–1185.
- 29 L. K. Frevel and H. W. Rinn, *Anal. Chem.*, 1955, 27, 1329–1330.
- 30 H. Schäfer, R. Gruehn and F. Schulte, *Angew. Chemie Int. Ed. English*, 1966, 5, 40–52.
- 31 J. M. Amarilla, B. Casai and E. Ruiz-Hitzky, *J. Mater. Chem.*, 1996, 6, 1005–1011.

- 32 L. E. A. Harold P. Klug, X-Ray Diffraction Procedures: For Polycrystalline and Amorphous Materials, 2nd Edition | Wiley, Wiley, 2nd edn., 1974.
- 33 G. Ischia, H. R. Wenk, L. Lutterotti and F. Berberich, *J. Appl. Crystallogr.*, 2005, **38**, 377–380.
- 34 R. Nasri, S. F. Chérif, M. F. Zid and A. Driss, *Acta Crystallogr. Sect. E Struct. Reports Online*, 2014, **70**, i20.
- 35 K. K. B. W. H. Schasow, H. Oppermann, O. Grossmann, *Cryst. Res. Technol.*, 1991, **4**, 401–407.
- 36 C. Bergner, V. Vashook, S. Leoni and H. Langbein, *J. Solid State Chem.*, 2009, **182**, 2053–2060.
- 37 A. Valentoni, P. Barra, N. Senes, G. Mulas, C. Pistidda, J. Bednarcik, F. Torre, S. Garroni and S. Enzo, *Dalt. Trans.*, 2019, **48**, 10986–10995.
- 38 J. Hidde, C. Guguschev and D. Klimm, *J. Cryst. Growth*, 2019, **509**, 60–65.
- 39 F. Gang, K. von Klinski-Wetzel, J. N. Wagner and M. Heilmaier, *Oxid. Met.*, 2014, **83**, 119–132.